



Glacier area changes in Novaya Zemlya from 1986-89 to 2019-21 using object-based image analysis in Google Earth Engine

Ali, A., Dunlop, P., Coleman, S., Kerr, D., McNabb, R., & Noormets, R. (2023). Glacier area changes in Novaya Zemlya from 1986-89 to 2019-21 using object-based image analysis in Google Earth Engine. *Journal of Glaciology*, 1-12. <https://doi.org/10.1017/jog.2023.18>

[Link to publication record in Ulster University Research Portal](#)

Published in:
Journal of Glaciology

Publication Status:
Published online: 09/05/2023

DOI:
<https://doi.org/10.1017/jog.2023.18>

Document Version
Author Accepted version

General rights
Copyright for the publications made accessible via Ulster University's Research Portal is retained by the author(s) and / or other copyright owners and it is a condition of accessing these publications that users recognise and abide by the legal requirements associated with these rights.

Take down policy
The Research Portal is Ulster University's institutional repository that provides access to Ulster's research outputs. Every effort has been made to ensure that content in the Research Portal does not infringe any person's rights, or applicable UK laws. If you discover content in the Research Portal that you believe breaches copyright or violates any law, please contact pure-support@ulster.ac.uk.

Glacier area changes in Novaya Zemlya from 1986-89 to 2019-21 using object-based image analysis in Google Earth Engine

Asim Ali¹, Paul Dunlop¹, Sonya Coleman,² Dermot Kerr², Robert W McNabb¹, Riko Noormets³

¹*School of Geography and Environmental Sciences, Ulster University, UK*

²*School of Computing, Engineering, and Intelligent Systems, Ulster University, UK*

³*School of Marine, Geology, and Geophysics, University Centre in Svalbard*

Correspondence: Asim Ali <ali-a18@ulster.ac.uk>

ABSTRACT. Climate change has had a significant impact on glacier recession, particularly in the Arctic, where glacier meltwater is an important contributor to global sea-level rise. Therefore, it is important to accurately quantify glacier recession within this sensitive region, using multiple observations of glacier extent. In this study, we mapped 480 glaciers in Novaya Zemlya, Russian Arctic, using object-based image analysis applied to multispectral Landsat satellite imagery in Google Earth Engine and quantify the area changes between 1986-89 to 2019-21. The results show that in 1986-89, the total glacierized area was $22\,990 \pm 301 \text{ km}^2$, in 2000-01 the area was $22\,525 \pm 308 \text{ km}^2$, and by 2019-21 the glacier area reduced to $21\,670 \pm 292 \text{ km}^2$, representing a total 5.8% reduction in glacier area between 1986-89 and 2019-21. Higher glacier area loss was observed on the Barents Sea coast (7.3%) compared to the Kara (4.2%), reflecting previously observed differences in warming trends. The accuracy of the automatically generated outlines of each layer (1986-89, 2000-01, and 2019-21) was evaluated by comparing with manually corrected outlines (reference data) using random sampling, resulting in an overall accuracy estimate of between 96% and 97% compared to the reference data. This automated approach in Google Earth Engine is a promising tool for rapidly mapping glacier change that reduces the amount of time required to generate accurate glacier

28 **outlines.**

29 INTRODUCTION

30 Glaciers distinct from the Antarctic and Greenland Ice Sheets are one of the key elements of the cryosphere
31 and are major freshwater reservoirs (Millan and others, 2022). As a result of climate change, these large
32 freshwater stores are now melting at a fast rate, increasing global sea levels (Hugonnet, Romain and 10
33 others, 2021; Zemp, M. and 14 others, 2019). After thermal expansion, glaciers and ice sheets are the
34 largest contributor to sea level rise in the 21st century (IPCC, 2021). With millions of people around
35 the world living within a few kilometres of the coast, future sea level rise has the potential to displace
36 populations across the globe (Kulp and Strauss, 2019).

37 Over the last few decades the rate of temperature increase in the Arctic has been estimated to be more
38 than twice as high as anywhere else in the world (Schädel, Christina and 14 others, 2018; You, Qinglong
39 and 15 others, 2021), with a recent study estimating Arctic warming to be as much as four times higher since
40 1979 (Rantanen, Mika and 7 others, 2022). In the Arctic, mountain glaciers, ice caps, and the Greenland
41 Ice Sheet (GrIS) have all retreated over the past 100 years and have started to retreat faster since 2000
42 (AMAP, 2017). Combined, Arctic glaciers, ice caps, and the GrIS contributed approximately 1.2 mm to
43 sea level rise each year from 2003 to 2015 (Moon, Twila A. and 14 others, 2019).

44 Given the importance of glaciers in the Arctic and their potential to impact large parts of the world,
45 it is necessary to develop automated methods that can easily monitor regional glacier changes and provide
46 a clear understanding of the climate change impacts on Arctic glaciers. To monitor changes over such an
47 expansive and largely inaccessible region like the Arctic, satellite remote sensing is an ideal tool as it can
48 be used to map large glacierized areas relatively quickly (e.g., Winsvold and others, 2014).

49 Several techniques have been used for glacier mapping based on remote sensing data, such as manual
50 delineation (e.g., Albert, 2002), band ratio (e.g., Bolch and others, 2010), Normalized Difference Snow Index
51 (NDSI) (Hall and others, 1995), object-based image analysis (e.g., Robson and others, 2015, 2016), and
52 supervised learning-based classification (e.g., Maximum likelihood, support vector machine, and random
53 forest; Khan and others, 2020; Kumar and others, 2021b; Nijhawan and others, 2016). Of these methods,
54 manual delineation is considered to be the most accurate (Albert, 2002; Alifu and others, 2015; Paul, 2017),
55 but this method is both time-consuming and potentially more susceptible to operator bias compared to

56 more automated approaches. Both band ratio and NDSI are well-established, fast, and robust methods
57 for mapping debris-free glacier ice over extensive areas (Paul, F. and 24 others, 2015). However, some
58 difficulties are still present in using these index-based methods - for example, mapping glaciers in the
59 presence of lakes, clouds, shadow, seasonal snow, and debris cover.

60 Band ratio with visible and Shortwave Infrared (SWIR) bands from Landsat imagery (red/SWIR1) is
61 an effective method for mapping shadowed ice, but tends to misclassify lakes (water bodies) as part of the
62 glacier (Kääb, A. M. and 11 others, 2005; Paul and others, 2007). Band ratio with Near Infrared (NIR)
63 and SWIR (NIR/SWIR1) have also been used, but using NIR with SWIR is less effective in areas with
64 dark shadows (Burns and Nolin, 2014). NDSI can provide more satisfactory results in the case of shaded
65 ice, but fails to differentiate glacier ice from pro-glacial lakes (Racoviteanu and others, 2008). Supervised
66 learning based classification techniques may have limited applicability over large regions because of the
67 longer processing time (Racoviteanu and others, 2009).

68 Glacier outlines are an important data source that not only tell us the size of the glacier, but importantly
69 are used for estimating ice volume (Millan and others, 2022) and glacier mass change (Zemp, M. and 14
70 others, 2019), or predicting sea level rise (Hock, R. and 7 others, 2019). The Randolph Glacier Inventory
71 (RGI) is a global inventory of glaciers, and it is supplementary to the Global Land Ice Measurements from
72 Space (GLIMS) database (RGI Consortium, 2017). GLIMS is an open-access digital database that stores
73 glacier outlines and is a cooperative effort of worldwide institutes (Raup and others, 2007), available at
74 <https://www.glims.org/>. However, for most glaciers around the world, outlines are only available at a
75 single point in time which limits its use for understanding the long term impacts of climate change for
76 glaciers in many regions.

77 In order to map glacier changes over large areas over multiple points in time, multiple satellite images are
78 needed. To do this mapping locally, users must download and store each image, with file sizes ranging from
79 ~200 MB for complete Landsat 4-5 scenes, to ~1 GB for Sentinel-2 or Landsat 8 and 9 scenes. Processing
80 large images on a desktop or laptop computer can be resource-intensive, which provides an additional cost
81 barrier for large-scale mapping efforts. More recently, cloud-based platforms such as Google Earth Engine
82 (Gorelick and others, 2017) have enabled users to forgo the time and costs of downloading, storing, and
83 processing images locally, which has greatly expanded the possibilities for large-scale analysis in a number
84 of fields (e.g., Zhang, Xiao and 6 others, 2020; Lea, 2018; Mahdianpari, Masoud and 7 others, 2020).

85 In this study, a method is developed on the Google Earth Engine cloud-based platform using an object-

86 based image analysis approach to map and generate glacier outlines automatically. We use this method
87 to generate multi-temporal outlines of glaciers on Novaya Zemlya, Russian Arctic. The main goals of this
88 study are: i) to develop an automated method to map glaciers by leveraging the computational power and
89 extensive data catalogue of Google Earth Engine; ii) to map the glaciers of Novaya Zemlya at multiple
90 points in time; iii) to compare the derived area changes to mass losses (Hugonnet, Romain and 10 others,
91 2021); and iv) to evaluate the accuracy of the method using manually-corrected outlines.

92 **STUDY AREA**

93 The Russian Arctic consists of three main regions: Franz Josef Land, Severnaya Zemlya, and Novaya
94 Zemlya, which lies north of the Russian mainland between the Barents and Kara Seas (Grant and others,
95 2009). According to the RGI version 6.0 (RGI 6.0), the glacier-covered area of Severnaya Zemlya is 16
96 701 km², for Franz Josef Land it is 12 762 km² and for Novaya Zemlya it is 22 128 km² (RGI Consortium,
97 2017). The most prominent feature of Novaya Zemlya is the large ice cap on the northern island (Severny
98 Island), whereas the southern part of the archipelago (Yuzhny Island) is dominated by small valley and
99 mountain glaciers (Melkonian and others, 2016). The ice cap on the northern side of Novaya Zemlya is
100 approximately 400 km long and has a maximum elevation of 1 600 m above sea level (a.s.l.), with the
101 southern part of Novaya Zemlya reaching 1 340 m a.s.l. (Rastner and others, 2017).

102 Novaya Zemlya (Fig. 1) has three different types of glaciers: the main ice cap's large outlet glaciers are
103 mostly marine-terminating, while most of the glaciers that are separated from the main ice cap are land-
104 terminating, with a small number of lake-terminating glaciers (Rastner and others, 2017). According to the
105 RGI 6.0, Novaya Zemlya has a total of 480 glaciers: 38 marine-terminating glaciers, 424 land-terminating
106 glaciers, and 18 lake-terminating glaciers.

107 **DATA AND METHODS**

108 **Data**

109 Landsat images have proven to be an effective asset for glacier mapping, and for creating multi-temporal
110 outlines of glaciers due to its large swath width, its multispectral capabilities, and its long temporal record
111 of capturing images over 5 decades (e.g., Nuth, C. and 7 others, 2013). A total of sixteen images from
112 Landsat 5 Thematic Mapper (TM), Landsat 7 Enhanced Thematic Mapper Plus (ETM+), and Landsat 8

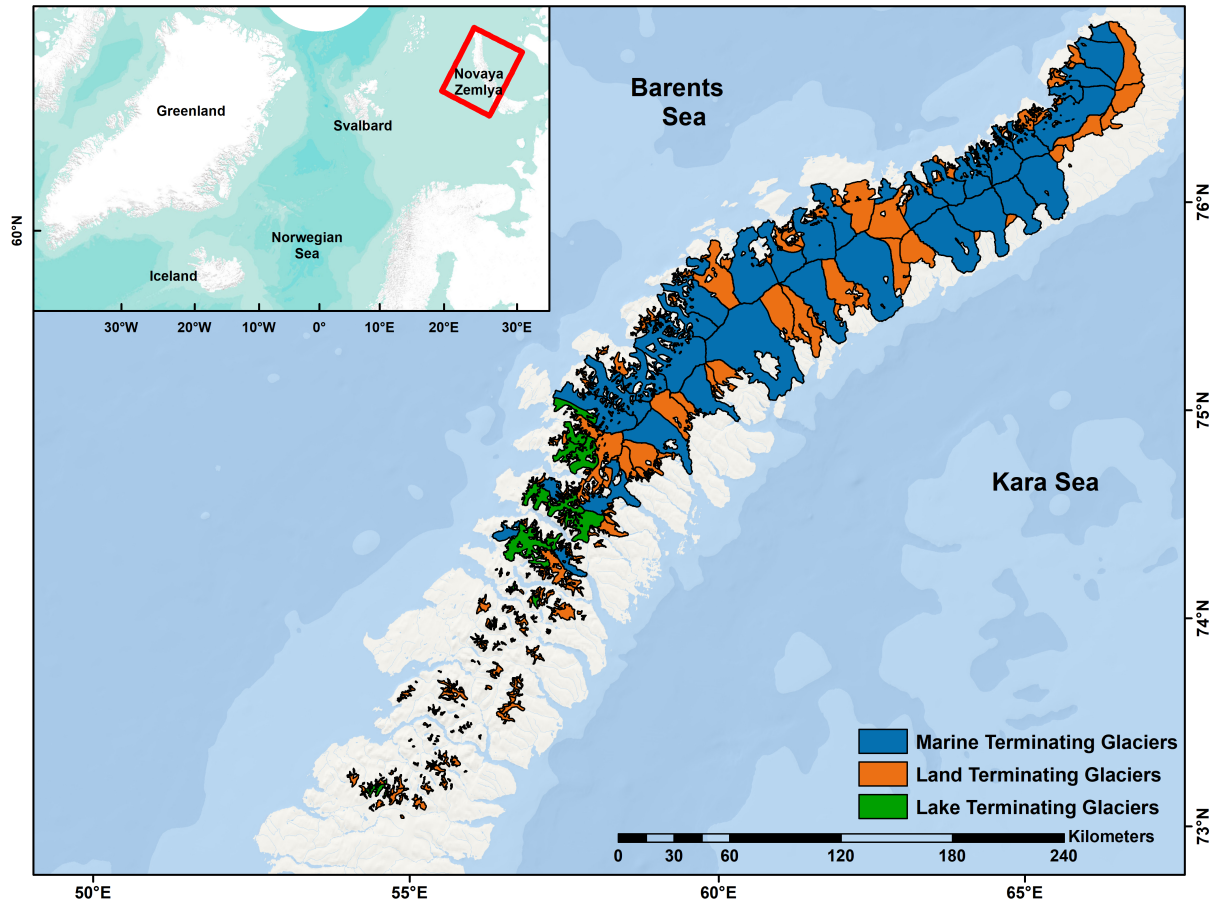


Fig. 1. The study area of Novaya Zemlya, with RGI 6.0 glacier outlines shown. The ESRI World Ocean and World Terrain basemaps are used in the background.

Table 1. Details of the Landsat images that are used in this study.

S. No	Satellite	Date (DD/MM/YYYY)	WRS-2 Path/Row	Google Earth Engine Image IDs
01	Landsat 5	26/07/1986	174/6	LANDSAT/LT05/C01/T1_SR/LT05_174006_19860726
02	Landsat 5	03/08/1987	177/6	LANDSAT/LT05/C01/T1_SR/LT05_177006_19870803
03	Landsat 5	06/08/1989	179/6	LANDSAT/LT05/C01/T1_SR/LT05_179006_19890806
04	Landsat 5	06/08/1989	179/7	LANDSAT/LT05/C01/T1_SR/LT05_179007_19890806
05	Landsat 5	06/08/1989	179/8	LANDSAT/LT05/C01/T1_SR/LT05_179008_19890806
06	Landsat 7	25/08/2000	174/6	LANDSAT/LE07/C01/T1_SR/LE07_174006_20000825
07	Landsat 7	31/07/2000	175/6	LANDSAT/LE07/C01/T1_SR/LE07_175006_20000731
08	Landsat 7	12/08/2000	179/6	LANDSAT/LE07/C01/T1_SR/LE07_179006_20000812
09	Landsat 7	12/08/2000	179/7	LANDSAT/LE07/C01/T1_SR/LE07_179007_20000812
10	Landsat 7	08/08/2001	178/8	LANDSAT/LE07/C01/T1_SR/LE07_178008_20010808
11	Landsat 8	20/08/2019	176/5	LANDSAT/LC08/C01/T1_SR/LC08_176005_20190820
12	Landsat 8	20/08/2019	176/6	LANDSAT/LC08/C01/T1_SR/LC08_176006_20190820
13	Landsat 8	23/08/2021	178/7	LANDSAT/LC08/C01/T1_SR/LC08_178007_20210823
14	Landsat 8	18/08/2020	180/6	LANDSAT/LC08/C01/T1_SR/LC08_180006_20200818
15	Landsat 8	19/09/2020	180/7	LANDSAT/LC08/C01/T1_SR/LC08_180007_20200919
16	Landsat 8	19/09/2020	180/8	LANDSAT/LC08/C01/T1_SR/LC08_180008_20200919

Operational Land Imager (OLI) are used in this study (Table 1), divided into three time periods: 1986-89, 2000-01, and 2019-21. The images used were carefully selected with minimal cloud cover.

Landsat is a collaborative effort of the USGS and NASA and has been continuously observing the Earth from 1972 until the present day (Wulder, Michael A. and 26 others, 2022). The USGS provides Landsat products in three categories: real-time (RT), Tier 1, and Tier 2 which are stored in Collection 1 or 2. Tier 1 images have the best quality, and are considered suitable for time-series analysis (Masek, Jeffrey G. and 6 others, 2020), while Tier 2 images have issues with geometric correction but are still usable. In this study, we use orthorectified Level-2 (surface reflectance) images (Tier 1) from Collection 1 for mapping glaciers in Novaya Zemlya. Some studies have used raw radiance or Digital Number (DN) values for glacier mapping with no atmospheric or topographic correction (Alifu and others, 2015; Paul and others, 2002). However, surface reflectance data is essential for systematic analysis, particularly in highly automated approaches (Hemati and others, 2021).

125 Method

126 Google Earth Engine is a cloud-based remote sensing platform with planetary-scale analysis capabilities
127 that contains a multi-petabyte catalogue of satellite imagery and geospatial datasets, making Google Earth
128 Engine one of the most powerful remote sensing analysis tools available for analysing change datasets
129 (Gorelick and others, 2017). Using Google Earth Engine, we developed an object-based image analysis
130 approach for classifying imagery, instead of a simpler pixel-based approach. Pixel-based classification
131 focuses on individual pixels and neglects additional contextual information contained in surrounding pixels
132 that could be used to increase the accuracy such as the spatial relationship with surrounding pixels, size
133 of objects, texture, and shape that object-based image analysis incorporates (Blaschke, 2010).

134 The method was initially developed using a single Landsat 8 OLI/TIRS image before being applied
135 to the other image sets for the whole of Novaya Zemlya to map glacier changes. This study utilizes six
136 bands from visible to SWIR (OLI Bands 2-7), and one thermal infrared band (TIR; TIRS Band 10) as
137 input layers for image segmentation (Fig. 2). The visible to SWIR bands have 30 m resolution. The TIR
138 band was originally collected with 100 m resolution, but Google Earth Engine automatically resampled
139 this using a cubic convolution method to 30 m.

140 In the object-based image analysis approach, segmentation is an important step that groups similar
141 pixels into a cluster or image objects (Ren and Malik, 2003). Pixel-based classification can result in so-
142 called “salt and pepper” noise, and segmentation helps to reduce this effect in the final classification (Ma
143 and others, 2019). To reduce noise in the images, a one-sigma Gaussian filter of radius 2 was applied before
144 segmentation (Xue, Xingyu and 7 others, 2018).

145 Google Earth Engine mainly supports three image segmentation techniques for remote sensing: simple
146 non-Iterative clustering, k-means, and G-means (Liu, Xiaoping and 7 others, 2018). We use simple non-
147 iterative clustering (Achanta and Ssstrunk, 2017), which is an improved version of simple linear clustering,
148 to segment the Landsat image (Fig. 3b). The important parameters of simple non-iterative clustering are
149 compactness, connectivity, seeds or grid size, and neighbourhood size. The compactness parameter defines
150 the smoothness of the clusters, which affects cluster shape (Shafizadeh-Moghadam and others, 2021). A
151 compactness value of zero removes spatial distance weighting, meaning that clusters are created based only
152 on spectral characteristics. The connectivity parameter deals with adjacent objects, with a connectivity
153 of 4 corresponding to only orthogonal neighbours, and a connectivity of 8 corresponding to orthogonal
154 and diagonal neighbours. The seed/size parameter determines the initial location or spacing of the cluster

155 centers, and neighbourhood size is used to avoid boundary artifacts between tiles (Tassi and Vizzari,
156 2020). In this study, the parameters compactness = 0, connectivity = 4, seed grid spacing of 15 pixels,
157 and neighbourhood size = 128 pixels were selected by repeated iteration and visual evaluation.

158 The Random Forest classifier was implemented in Google Earth Engine for the classification of the
159 segmented image. The Random Forest algorithm is a supervised machine learning algorithm that combines
160 the output of multiple decision trees to produce a single result (Kulkarni and Lowe, 2016). For image
161 classification, Random Forest is the most widely used machine learning algorithm in Google Earth Engine
162 (Amani, Meisam and 11 others, 2020). Random Forest is robust, easier to implement, capable of dealing
163 with high dimensionality, and can reduce the risk of overfitting (Nery and others, 2016; Praticò and others,
164 2021).

165 In this study, the Random Forest algorithm using ten trees was trained on manually selected samples
166 of “glacier” and “non-glacier” throughout the scene, and the segments were classified into two main classes:
167 “glacier” and “non-glacier”. The “glacier” class includes ice, debris-covered ice, and moraines, while the
168 non-glacier class includes water, vegetation, sea-ice, bare land and seasonal snow patches. To train the
169 classifier, we used a total of 620 samples for the 1986-89 images, including 365 glacier samples and 363
170 non-glacier samples. For the 2000-01 images, we used 317 glacier and 303 non-glacier samples, and for the
171 2019-21 images we used 339 glacier and 367 non-glacier samples.

172 Finally, a median filter with radius 2.5 was applied to reduce noise in the classified image, and the
173 classified image was converted from raster to vector to create glacier outlines (Fig. 3c). The automated
174 glacier outlines were exported from Google Earth Engine to ArcMap 10.5.1 for post processing. As a final
175 step, each glacier was visually examined to see if manual correction was required, and manual corrections
176 were made where necessary. Finally, the linked glacier outlines were separated using the internal boundaries
177 of the RGI 6.0, to enable examination of the changes in each glacier.

178 **Accuracy and Uncertainty**

179 The temporal nature by which satellite images are captured invariably means that images of the same area
180 are captured during different conditions, and there can be seasonal variations that can impact on image
181 quality. These variations can be illumination differences, cloud cover, or shadows cast over the target
182 feature; for glacier mapping, seasonal snow patches can remain on the ground which are spectrally similar
183 to snow-covered glaciers. Because of this, it is important to understand the capabilities of the method

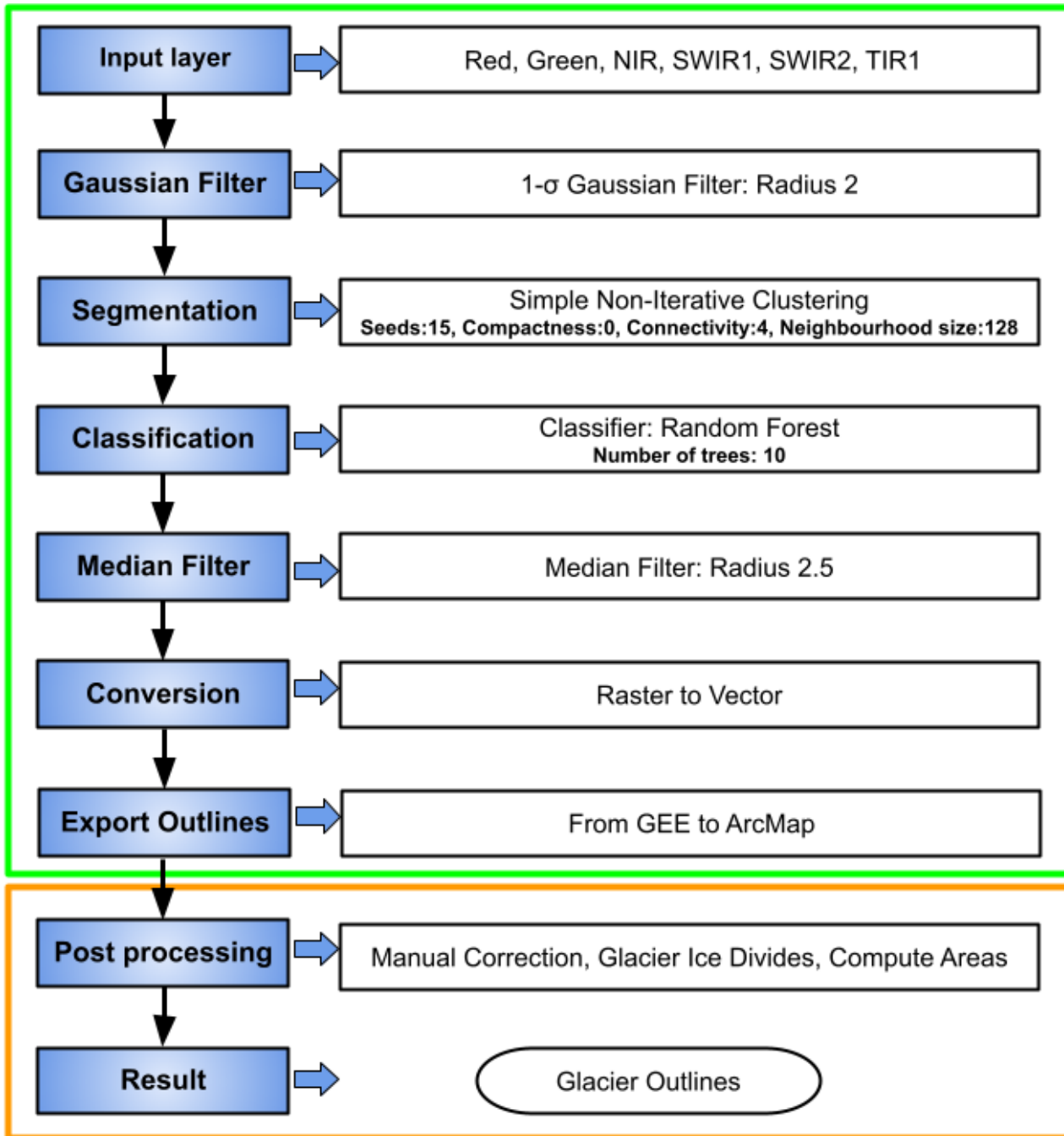


Fig. 2. Workflow of the method for creating glacier outlines in Google Earth Engine. The green box shows the automated steps in Google Earth Engine, while the orange box shows the post-processing steps in ArcMap 10.5.1.

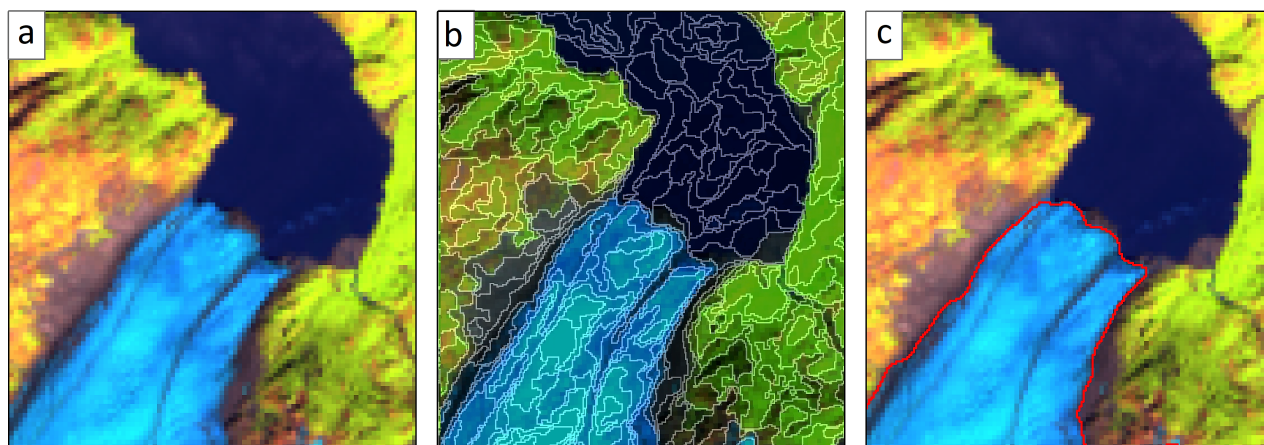


Fig. 3. The process of generating outlines using an object-based image analysis approach in Google Earth Engine: (a) a false colour composite of a Landsat 8 image (OLI Bands SWIR1, NIR, and Red); (b) the result of simple non-Iterative clustering segmentation; (c) the final glacier outline, overlain on the original image.

184 when utilising images from different times and to assess how accurate the glacier areas are computed using
185 this automated methodology without manual corrections. Therefore, to determine the uncertainty in the
186 glacier area, two approaches were used: random sampling and buffer analysis.

187 **Uncertainty by random sampling**

188 To assess the accuracy of the automated outlines from each period, random samples were generated for
189 each class in ArcMap 10.5.1, using the manually corrected outlines as reference data. The random samples
190 were separated into two classes: “glacier” and “non-glacier”, with an equal number of samples for each
191 class. In total, 1 998 samples for each class were taken for the 1986-89 outlines; 1 971 samples from each
192 class for the 2000-01 outlines; and 1 937 samples from each class for the 2019-21 outlines. These points
193 were intersected with the automatically generated outlines and the reference data, and confusion matrices
194 were created (Table 2).

195 **Uncertainty using buffer analysis**

196 To assess the area uncertainty of the manually-corrected outlines, a buffer of ± 30 m was applied to each
197 manually corrected layer. In the absence of suitable reference data, the buffer approach is typically employed
198 to determine accuracy using a literature-derived uncertainty value (± 0.5 or 1 pixel; Granshaw and Fountain,
199 2006; Paul, F. and 10 others, 2017). The uncertainty in the glacier area was determined by calculating
200 the buffered area of each layer. The high, low, and area \pm uncertainty values for each period are shown in

Table 2. Confusion matrices of each layer generated based on random sampling

1986-89		Reference Data				
		Glacier	Non-glacier	Total	User's accuracy	Kappa
Classified	Glacier	1 973	100	2 073	95.1%	0.93
	Non-glacier	25	1 898	1 923	98.7%	
	Total	1 998	1 998	3 996		
	Producer's accuracy	98.7%	94.9%			
2000-01		Reference Data				
		Glacier	Non-glacier	Total	User's accuracy	Kappa
Classified	Glacier	1 954	140	2 094	93.3%	0.92
	Non-glacier	17	1 831	1 848	99.0%	
	Total	1 971	1 971	3 942		
	Producer's accuracy	99.1%	92.8%			
2019-21		Reference Data				
		Glacier	Non-glacier	Total	User's accuracy	Kappa
Classified	Glacier	1 917	115	2 032	94.3%	0.93
	Non-glacier	20	1 822	1 842	98.9%	
	Total	1 937	1 937	3 874		
	Producer's accuracy	98.9%	94.0%			

Table 3. Computed areas (in km²) of each layer based on the ± 30 m buffer

Time period	High	Low	Area
1986-89	23 291	22 689	22 990 \pm 301
2000-01	22 833	22 217	22 525 \pm 308
2019-21	21 962	21 378	21 670 \pm 292

201 Table 3.

202 RESULTS

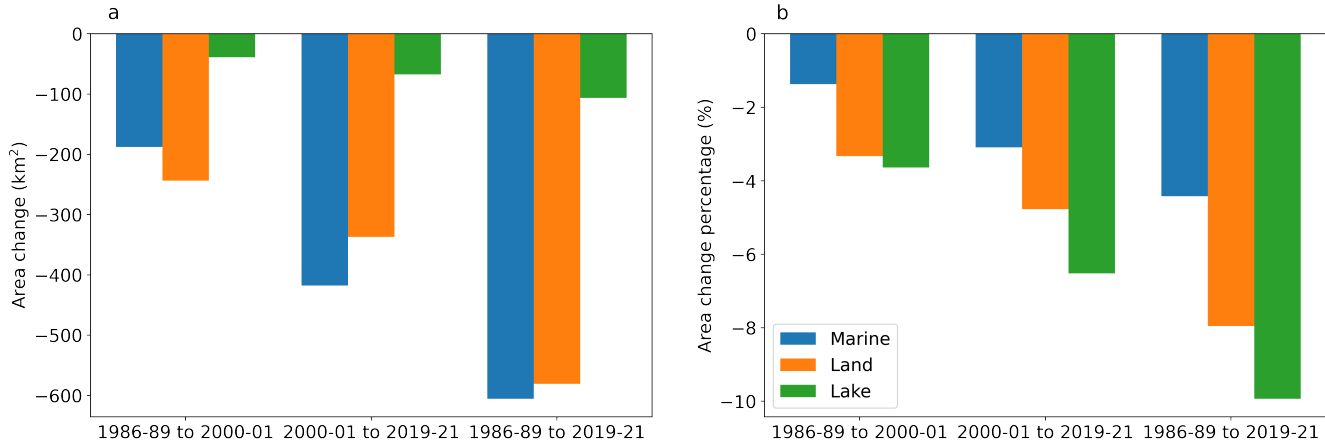
203 In 1986-89, the total glacierized region of Novaya Zemlya was 22 990 \pm 301 km², in 2000-01 the area was 22
 204 525 \pm 308 km², and by 2019-21 the glacier area was reduced to 21 670 \pm 292 km². Of the 480 glaciers mapped,
 205 142 are greater than 10 km², 262 glaciers are between 1 to 10 km², and 76 glacier are smaller than 1 km².
 206 This glacier inventory includes three terminus types: 38 marine-terminating, 424 land-terminating, and 18
 207 lake-terminating glaciers. The marine-terminating glaciers cover the most glacier area (14 448 \pm 137 km²),
 208 followed by the land-terminating glaciers covering 7 299 \pm 94 km², and the lake-terminating glaciers that
 209 cover 1 241 \pm 16 km².

210 The overall accuracy for each layer was calculated using the confusion matrices (Table 2). The 1986-89
 211 layer showed 96.8% overall accuracy, the 2000-01 layer had 96.0% accuracy, and the 2019-21 layer had
 212 96.5% accuracy. The details of producer's and user's accuracy are mentioned in Table 2. The producer's
 213 accuracy varies between 92.8% and 98.9%, the user's accuracy ranges between 93.3% and 99.0%, and the
 214 kappa coefficient is greater or equal to 0.92 for all three layers.

215 It is also important to assess how accurate the automatically-generated glacier areas are, using the
 216 information displayed in Table 2. Table 4 compares the manually estimated glacier areas with the unbiased
 217 estimates of glacier area for each time period, calculated following the methods described by Olofsson and
 218 others (2013). The comparison of manual and automated area estimates shows that besides 2000-01, the
 219 manual and automated area estimates overlap within the uncertainty bands. When compared to 1986-
 220 89 and 2000-01, the manual area estimate shows that the area loss nearly doubled between 2000-01 and
 221 2019-21, whereas the automatic estimate shows the opposite. Additionally, the automated estimate of the
 222 area change between 2000-01 and 2019-21 has a larger uncertainty (± 624 km²) than the estimated change
 223 (-441 km²).

Table 4. The total area (in km²) of glaciers computed from manually corrected outlines (± 1 pixel buffer), both including and excluding glaciers that surged, and the automatically generated outlines ($\pm 95\%$ confidence interval)

	Manual		Change (from previous)		Automated	Change (from previous)
	All	Non-Surge	All	Non-Surge		
1986-89	22 990 \pm 301	22 049 \pm 301			22 930 \pm 470	
2000-01	22 525 \pm 308	21 578 \pm 308	-465 \pm 430	-470 \pm 430	21 762 \pm 435	-1 168 \pm 640
2019-21	21 670 \pm 292	20 756 \pm 292	-855 \pm 424	-821 \pm 424	21 321 \pm 448	-441 \pm 624

**Fig. 4.** The total area change for lake, marine, and land-terminating glaciers in both km² (a) and percent area (b).

224 Glacier area changes

225 To calculate area changes, we use the manually-corrected glacier outlines. Between 1986-89 and 2019-2021,
 226 glaciers in Novaya Zemlya showed a 5.8% reduction in total area. Glacier retreat rates increased by 1.7%
 227 from 2000-01 to 2019-21 (-3.8%), compared to 1986-89 to 2000-01 (-2.1%). These changes in glacier area
 228 were not constant across glacier terminus type (land, lake, and marine-terminating). From 1986-89 to
 229 2019-21, land-terminating glaciers lost 580 ± 130 km² (7.9%), lake-terminating glaciers lost 106 ± 21 km²
 230 (9.9%), and marine-terminating glaciers lost 605 ± 263 km² (4.4%) of glacierized area Fig. 4.

231 Fig. 5a depicts the area lost for each glacier from 1986-89 to 2000-01 and Fig. 5b shows the loss of each
 232 glacier from 2000-01 to 2019-21, while Fig. 5c and 5d show the area loss of each glacier as a percentage.
 233 Only 41 glaciers larger than 200 km² are responsible for nearly half (49.5%) of the area loss in the region,
 234 and 272 glaciers are responsible for 84% of the total glacier area loss. Because of the larger area of these
 235 glaciers, however, the total percentage loss for these 272 glaciers is less than 25%.

236 Fig. 6 shows the percent area change vs glacier area based on terminus type. Fig. 6b depicts 38

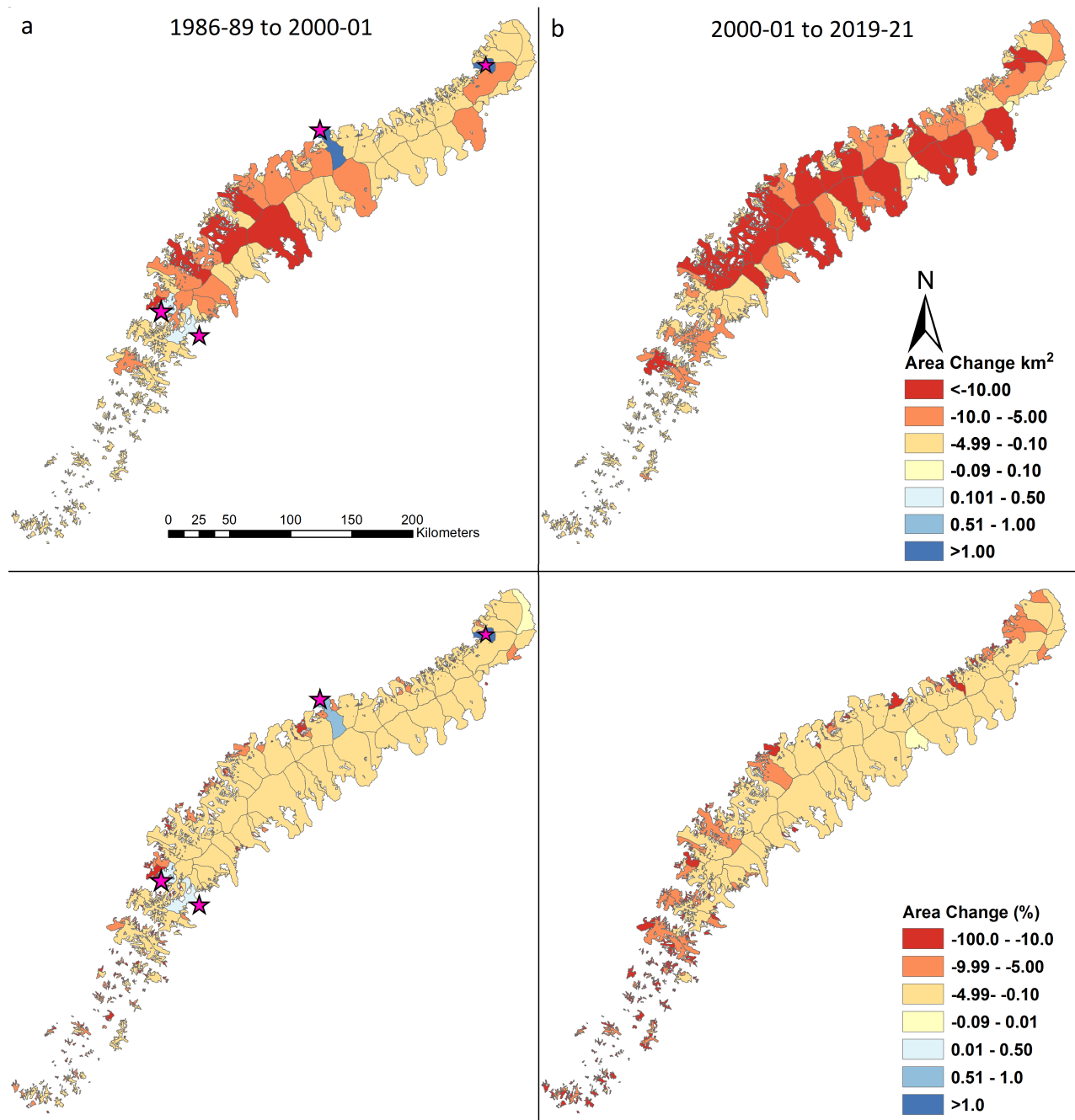


Fig. 5. Area changes of Novaya Zemlya glaciers, (a) from 1986-89 to 2000-01 and (b) 2000-01 to 2019-21 in km², and (c) from 1986-89 to 2000-01 and (d) 2000-01 to 2019-21 as a percent. Stars in a and c show glaciers that surged during the 1986-89 and 2000-01 period.

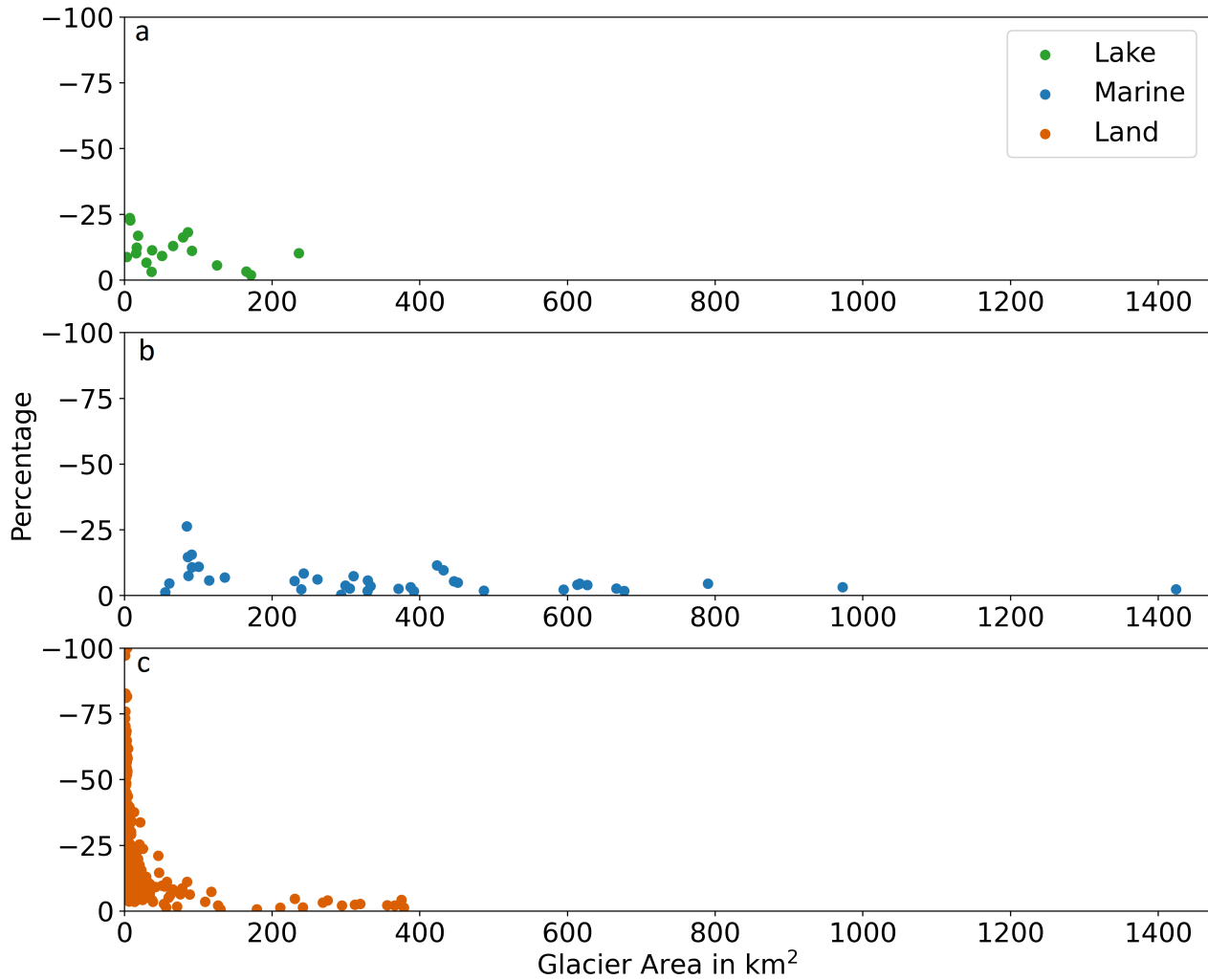


Fig. 6. Percent area change vs glacier area for each glacier from 1986-89 to 2019-21, for (a) lake-terminating, (b) marine-terminating, and (c) land-terminating glaciers.

237 marine-terminating glaciers that cover the majority of the glacierized region ($14\,448 \pm 137 \text{ km}^2$) in Novaya
 238 Zemlya, Fig. 6a shows 18 lake-terminating glaciers which cover $1\,241 \pm 16 \text{ km}^2$, while Fig. 6c shows 424
 239 land-terminating glaciers covering $7\,299 \pm 94 \text{ km}^2$. In between 1986-89 and 2019-21, three land-terminating
 240 glaciers have completely disappeared, and 18 glaciers retreated more than 60%, while a further 57 glaciers
 241 retreated between 40% and 60%.

242 DISCUSSION

243 Glacier retreat

244 As reported elsewhere (e.g., Sharp, Martin and 12 others, 2014; Kochtitzky and Copland, 2022), it is clear
245 that glaciers are retreating across the Arctic. This study shows that all glaciers in Novaya Zemlya have
246 retreated at various rates from 0.3% to 100%, with a few examples of surging glaciers captured in the
247 analysis (Fig. 5a,c). Although the area loss of glaciers differed by each glacier type in Novaya Zemlya.
248 Carr and others (2017) found that the retreat rate of marine-terminating glaciers is higher than that of
249 land-terminating glaciers, which is corroborated by our results (Fig. 4). However, land-terminating glaciers
250 did not experience the same increase in retreat rate as lake and marine-terminating glaciers in 2000-01 to
251 2019-21. The retreat rate of land-terminating glaciers increased by 1.4% between 2000-01 and 2019-21
252 relative to that between 1986-89 to 2000-01, whereas the retreat rates of lake- and marine-terminating
253 glaciers increased by 2.8% and 1.7%, respectively.

254 Like the rest of the Arctic, Novaya Zemlya is warming faster than the rest of the world, with both
255 surface air and sea surface temperatures increasing rapidly over both the Barents and Kara Sea coasts
256 (e.g., Kohnemann and others, 2017; Isaksen, Ketil and 15 others, 2022). In particular, Isaksen, Ketil and
257 15 others (2022) found that 2 m surface air temperature warming was higher on the Barents Sea side
258 of Novaya Zemlya ($1.5\text{--}2.0^{\circ}\text{C decade}^{-1}$ between 1981-2020) compared to the Kara Sea side ($1.0\text{--}1.5^{\circ}\text{C}$
259 decade^{-1}). These changes are driven in part by a decrease in sea ice concentration (SIC) in the region
260 (Yamagami and others, 2022), with the drop in SIC over the Barents Sea nearly twice as high compared
261 to the Kara Sea (Kumar and others, 2021a). Consistent with these studies, our observations show that
262 glaciers terminating on the Barents Sea coast of Novaya Zemlya retreated faster than glaciers terminating
263 on the Kara Sea coast (Fig. 7), a pattern that remains consistent across glacier terminus type (Fig. 8).
264 Barents Sea glaciers lost a total area of 843.4 km^2 (-7.3%) between 1986-89 and 2019-21, while glaciers on
265 the Kara Sea lost 448.9 km^2 (-4.2%).

266 Examination based on terminus type shows that all three types of glaciers are retreating more on the
267 Barents Sea side than those terminating on Kara Sea side (Fig. 8). Carr and others (2014) observed a similar
268 pattern of higher retreat on the Barents Sea coast than the Kara Sea between 1992 and 2010. Marine and
269 lake-terminating glaciers are retreating faster on both sides, in both time periods of the study, although
270 land-terminating glacier retreat is slowing down at the Barents Sea in 2000-01 to 2019-21 compared to

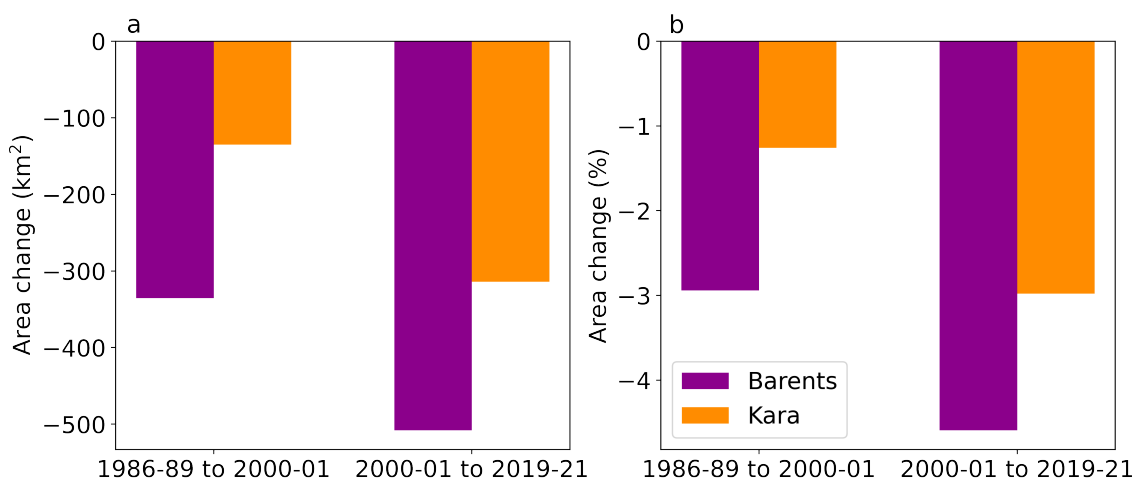


Fig. 7. Area change for glaciers on the Barents Sea vs Kara Sea (a) in km² and (b) as a percentage.

271 1986-89 and 2000-01.

272 All three types of glaciers: lake, marine, and land-terminating have lost more glacier area from 2000-
 273 01 to 2019-21 than 1986-89 to 2000-01; although, during the period 1986-89 to 2000-01, three marine-
 274 terminating glaciers and one lake-terminating glacier surged. Two of the same glaciers were identified
 275 by Carr and others (2017), and one was identified by Grant and others (2009). This study identified one
 276 additional glacier surge (Pavlov Glacier, RGI 6.0 ID: RGI60-09.00070) that increased the area of the glacier
 277 by 3.2 km², and showed terminus advance by up to 1.3 km by 2000-01 compared to 1986-89 (Fig. 9). No
 278 glacier surges were observed in the land-terminating glaciers. During 1986-89 to 2000-01, all four surged
 279 glaciers increased in area by 0.6% (+5.8 km²), however during the second time period (2000-01 to 2019-21),
 280 the same glaciers retreated and showed a strongly negative change in area of -3.4% (-32.6 km²), with a net
 281 area loss between 1986-89 and 2019-21 for each glacier. These four glacier were excluded from the area
 282 change analysis.

283 Comparison of glacier area loss with mass balance loss

284 Comparing glacier area changes with geodetic mass balances obtained from Hugonnet, Romain and 10
 285 others (2021) for the period 2000-2020 shows that marine-terminating glaciers lost both area (3.1%) as well
 286 as mass (-0.25 m a⁻¹) and lake-terminating glaciers lost a total of 6.5% area while also showing greater mass
 287 loss (-0.42 m a⁻¹) compared to land and marine terminating glaciers (Fig. 10). However, land-terminating
 288 glaciers show a slightly different pattern than lake and marine-terminating glaciers (Fig. 10), with land-
 289 terminating glaciers losing a substantial amount of area (4.7%) with less substantial mass loss (-0.18 m a⁻¹).

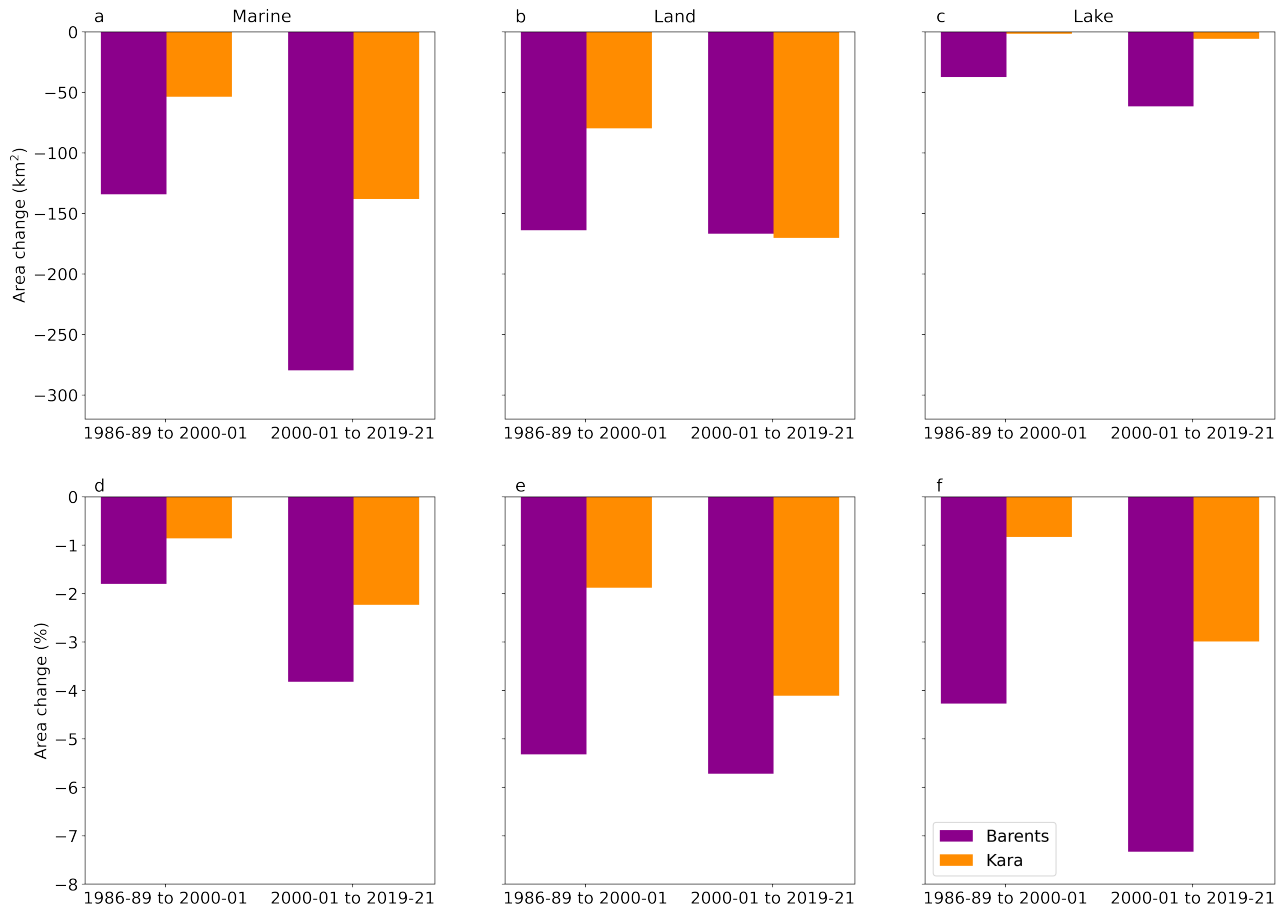


Fig. 8. Area change of marine (a, d), land (b, e) and lake-terminating (c, f) glaciers on the Barents Sea vs Kara Sea, in km^2 (a-c) and percent area (d-f).

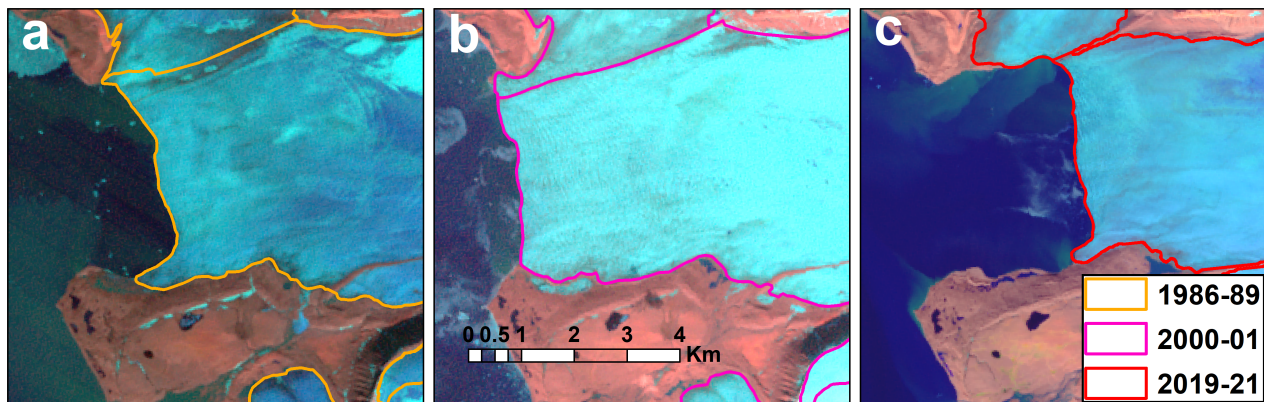


Fig. 9. Time series of Landsat images showing Pavlov Glacier (RGI60-09.00070) in (a) 1986-07-26, (b) 2000-07-31, and (c) 2019-08-20, showing a clear advance associated with a surge between 1986 and 2000.

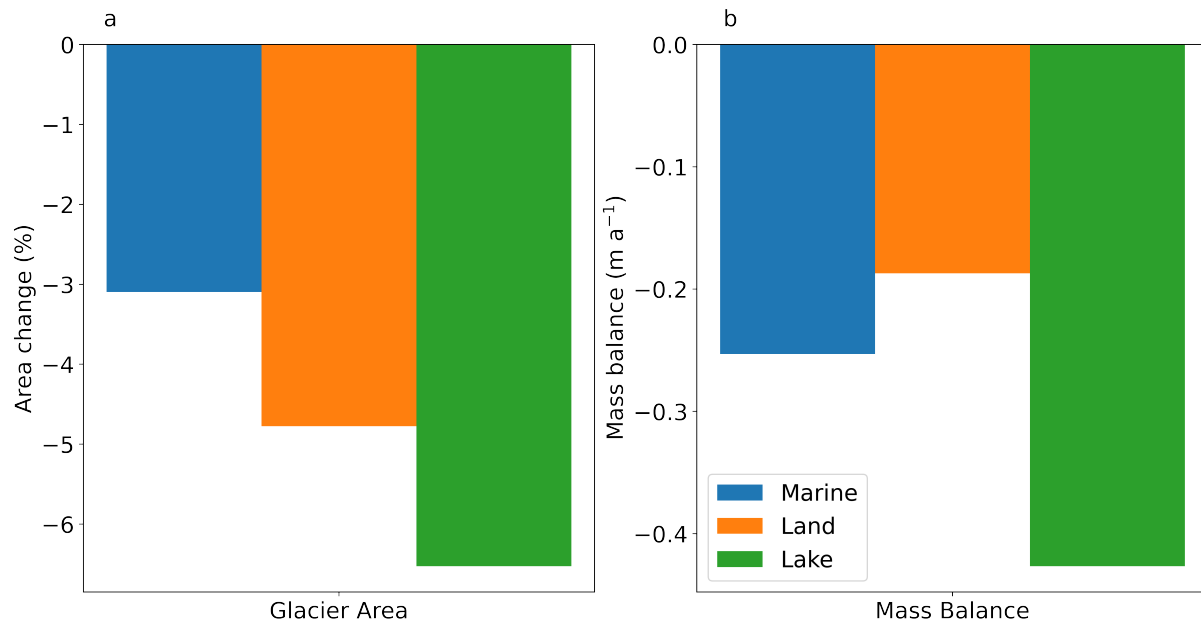


Fig. 10. (a) Percent area change (2000-01 to 2019-21) and (b) area-averaged mass change (2000-2020) from Hugonnet, Romain and 10 others (2021) for each glacier type.

290 Fig. 11 depicts a comparison of each glacier area loss with its mass loss. The results indicate that
 291 lake-terminating glaciers lost more area than land and marine-terminating glaciers (Fig. 10), with a more
 292 negative mass balance (Fig. 11). Ciraci and others (2018) found that marine-terminating glaciers are
 293 losing mass faster than glaciers terminating on land. Almost the same trend can be seen in marine-
 294 terminating glaciers, with a more more negative area-averaged mass balance for marine-terminating glaciers
 295 compared to land-terminating glaciers (Fig. 11), because marine and lake-terminating glaciers lose mass
 296 via frontal ablation and land-terminating glaciers do not. Land-terminating glaciers showed the least mass
 297 loss compared to marine and lake-terminating glaciers, as seen in the total mass loss of land-terminating
 298 glaciers (Fig. 10). In terms of relative area change, however, land-terminating glaciers showed a stronger
 299 decrease in area compared to marine-terminating glaciers.

300 Methodology framework in Google Earth Engine

301 Rastner and others (2013) compared object-based image analysis with pixel-based classification using the
 302 Red/SWIR band ratio technique, demonstrating that object-based image analysis performed better than
 303 pixel-based classification and reduced the time needed for manual corrections, despite the longer processing
 304 time required.

305 The 16 Level-2 products used in this study total 9.10 GB as distributed by USGS Earth Explorer.

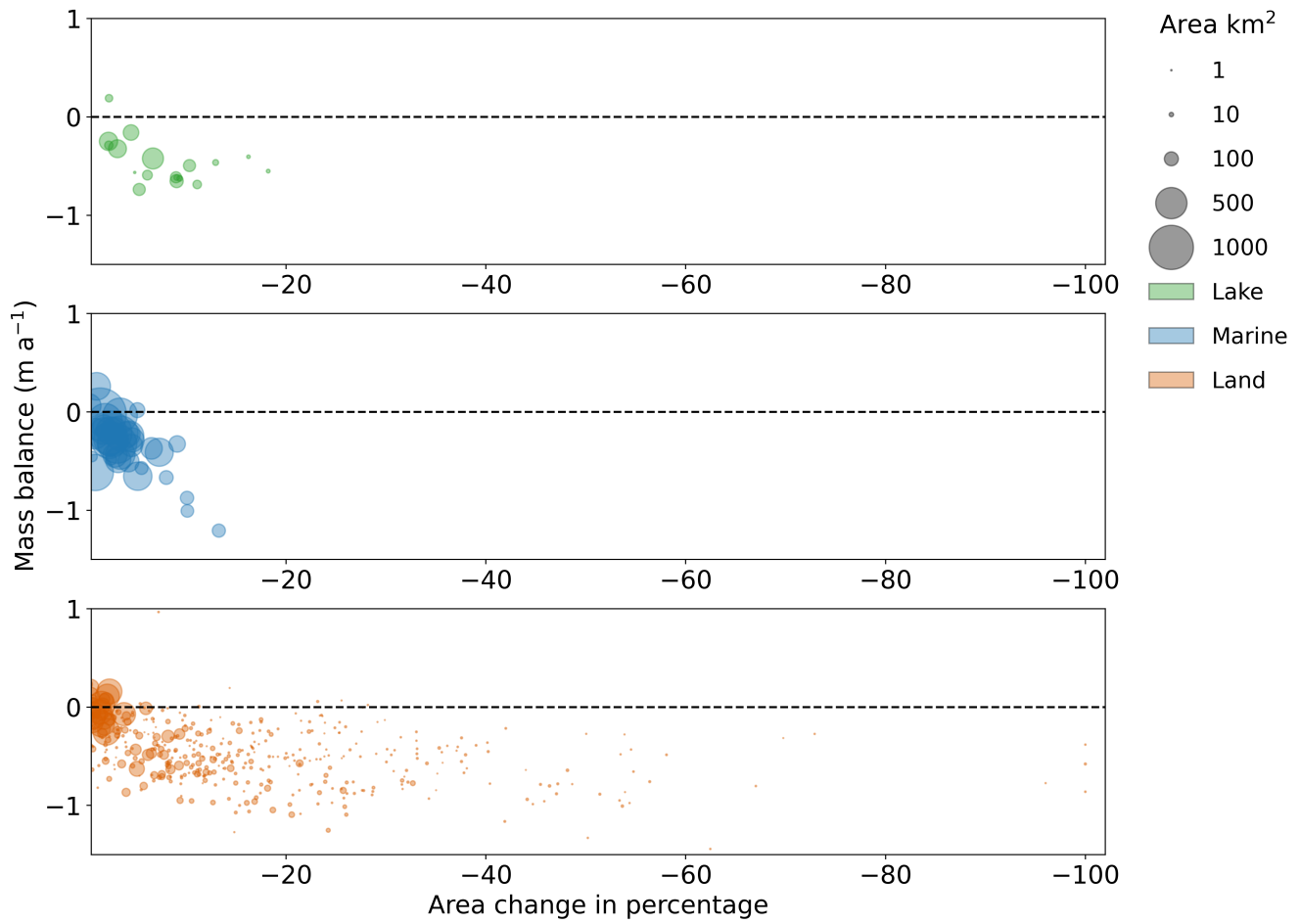


Fig. 11. Area-averaged mass change (2000-2020) from Hugonnet, Romain and 10 others (2021) vs percent area change (2000-01 to 2019-21) for each glacier.

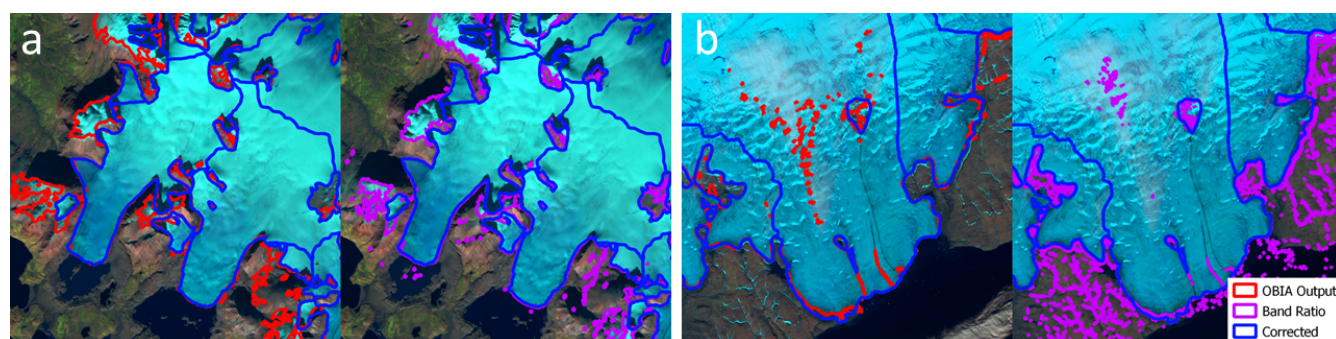


Fig. 12. Comparison between object-based image analysis, Band Ratio, and Corrected outlines for two different sites in Novaya Zemlya.

306 Downloading the files via the USGS Bulk Download Web Application took approximately 15 minutes,
307 even on a fast internet connection. In comparison, running the script to generate outlines for a single
308 image on Google Earth Engine and exporting the outlines took approximately one minute.

309 In addition to the time saved by forgoing downloading and processing the images locally, the object-
310 based image analysis method implemented on Google Earth Engine reduced the amount of manual correc-
311 tion needed when compared to the Red/SWIR1 band ratio method. Fig. 12 compares the object-based
312 image analysis output to the manually-corrected outlines, as well as the output of the Red/SWIR1 band
313 ratio using a threshold of 2.0, following Rastner and others (2017). Both outputs clearly require manual
314 correction, with large areas of seasonal snow captured by both methods in the area shown in Fig. 12a, but
315 the band ratio output captures a large area of seasonal and perennial snow patches (Fig. 12b) that is not
316 captured by the object-based image analysis output. In addition, both methods have misclassified areas of
317 thin cloud cover, shown in the middle of Fig. 12b, as well as areas with larger medial moraines.

318 In this study, the Google Earth Engine object-based image analysis approach removes the time required
319 for downloading, extracting, and storing the images, is easily applicable to other regions, and reduces the
320 amount of manual correction required, as compared to pixel-based methods. This method, however, may
321 not be effective for mapping debris-covered glaciers, or areas covered by fresh snow or thin cloud cover. To
322 address these issues, other approaches that have used object-based image analysis have included additional
323 datasets such as digital elevation models and terrain slope or coherence derived from synthetic aperture
324 radar (SAR) images (Robson and others, 2015, 2016). Unfortunately, many of these products are not yet
325 available in Google Earth Engine, though the possibility exists for users to upload and make use of these
326 additional datasets in their workflows.

327 **CONCLUSION**

328 This study presents a new object-based image analysis methodology, implemented in Google Earth Engine,
329 for rapid and accurate glacier mapping. The software framework designed in Google Earth Engine utilises
330 multi-temporal Landsat satellite imagery, and the outlines generated showed an accuracy of between 96%
331 and 97% when compared to a manually-corrected reference dataset. This demonstrates that our method-
332 ology is a powerful, robust tool for accurate and rapid mapping of glaciers changes on regional scale that
333 reducing the time required of manual correction and can be applied to other glacierized regions. Utilizing
334 this automated approach, we created outlines of glaciers on Novaya Zemlya for three different time periods:
335 1986-89, 2000-01, and 2019-21. This important dataset is essential for understanding the impact of climate
336 change on glaciers, and could be used to estimate ice volume and mass change.

337 This method allowed for a comprehensive analysis of the changes that occurred in Novaya Zemlya
338 glaciers between 1986-1989 and 2019-21. Over this time period, glaciers in Novaya Zemlya lost a total area
339 of $1\,292 \pm 419$ km² (5.8%), with three glaciers disappearing entirely. The results clearly demonstrate that
340 all glaciers in Novaya Zemlya are responding to the impacts of climatic warming in the Arctic. With the
341 exception of four glaciers that surged between 1986-89 to 2000-01, all glaciers in the study area retreated
342 between 1986-89 and 2019-21, and even those four glaciers have retreated since 2000-01.

343 Our analysis indicates there are regional variations in how glaciers are responding to oceanic warming
344 in this part of the Arctic, with more loss observed from glaciers that terminate on the Barents Sea side
345 of Novaya Zemlya compared to those that terminate on the Kara Sea side. In comparison, results showed
346 that land-terminating glaciers retreated less between 2000-01 and 2019-21 compared to 1986-89 to 2000-01,
347 while the retreat rate of marine-terminating glaciers increased from 2000-01 to 2019-21, relative to 1986-89
348 to 2000-01. While marine-terminating glaciers, which cover the majority of Novaya Zemlya, lost more area
349 than land and lake-terminating glaciers, lake-terminating glaciers showed a larger percentage loss than the
350 land and marine-terminating glaciers.

351 Detailed regional studies of glacier behaviour across the Arctic are important for understanding the
352 decadal responses and the likely trajectory of Arctic glaciers in a warming world. Given their potential
353 contribution to global sea levels it is important to map and understand the scale of change accurately and
354 to provide tools for rapid assessment at regional scales. Platforms such as Google Earth Engine, combined
355 with the expansive Landsat archive and approaches such as Object-Based Image Analysis, help provide

356 these tools.

357 DATA AND CODE AVAILABILITY

358 The manually corrected glacier outlines are available from the Global Land Ice Measurements from Space
359 (GLIMS) database at <http://www.glims.org/>. An example Google Earth Engine script demonstrating the
360 object-based image analysis process can be accessed at the following link:

361 https://code.earthengine.google.com/?accept_repo=users/buner_shapfile/OBIA_Example_code.

362 AUTHOR CONTRIBUTIONS

363 AA developed the method, performed data analysis and interpretation, created figures, and wrote the
364 initial draft of the manuscript. PD, SC, DK, and RM helped with conceptualization, methods, analysis,
365 and editing. RM also assisted with developing the method, creating figures, and interpretation. RN helped
366 with writing and editing the manuscript. All authors reviewed results and approved the final version of
367 the manuscript.

368 ACKNOWLEDGEMENTS

369 This work was carried out as part of Asim Ali's PhD project, funded by an Ulster University Vice Chan-
370 cellor's Research Studentship. Landsat images used in Google Earth Engine were provided courtesy of the
371 U.S. Geological Survey. We wish to thank James Lea, two anonymous reviewers, and the editors for their
372 constructive and insightful comments, which helped improve the quality of the manuscript.

373 REFERENCES

- 374 Achanta R and Ssstrunk S (2017) Superpixels and Polygons Using Simple Non-iterative Clustering. In *2017 IEEE*
375 *Conference on Computer Vision and Pattern Recognition (CVPR)*, 4895–4904 (doi: 10.1109/CVPR.2017.520)
- 376 Albert TH (2002) Evaluation of Remote Sensing Techniques for Ice-Area Classification Applied to the Tropical
377 Quelccaya Ice Cap, Peru. *Polar Geogr.*, **26**(3), 210–226 (doi: 10.1080/789610193)
- 378 Alifu H, Tateishi R and Johnson B (2015) A new band ratio technique for mapping debris-covered glaciers
379 using Landsat imagery and a digital elevation model. *Int. J. Remote Sens.*, **36**(8), 2063–2075 (doi:
380 10.1080/2150704X.2015.1034886)

- 381 Amani, Meisam and 11 others (2020) Google Earth Engine Cloud Computing Platform for Remote Sensing Big Data
382 Applications: A Comprehensive Review. *IEEE J. Sel. Top. Appl. Earth Obs. Remote Sens.*, **13**, 5326–5350 (doi:
383 10.1109/JSTARS.2020.3021052)
- 384 AMAP (2017) *Snow, Water, Ice and Permafrost in the Arctic (SWIPA) 2017*. Arctic Monitoring and Assessment
385 Programme (AMAP), ISBN 978-82-7971-101-8
- 386 Blaschke T (2010) Object based image analysis for remote sensing. *ISPRS J. Photogramm. Remote Sens.*, **65**(1),
387 2–16 (doi: 10.1016/j.isprsjprs.2009.06.004)
- 388 Bolch T, Menounos B and Wheate R (2010) Landsat-based inventory of glaciers in western Canada, 1985–2005.
389 *Remote Sens. Environ.*, **114**(1), 127–137 (doi: 10.1016/j.rse.2009.08.015)
- 390 Burns P and Nolin A (2014) Using atmospherically-corrected Landsat imagery to measure glacier area change in the
391 Cordillera Blanca, Peru from 1987 to 2010. *Remote Sens. Environ.*, **140**, 165–178 (doi: 10.1016/j.rse.2013.08.026)
- 392 Carr JR, Stokes CR and Vieli A (2014) Recent retreat of major outlet glaciers on Novaya Zemlya, Russian Arctic,
393 influenced by fjord geometry and sea-ice conditions. *J. Glaciol.*, **60**(219), 155–170 (doi: 10.3189/2014JøG13J122)
- 394 Carr JR, Bell H, Killick R and Holt T (2017) Exceptional retreat of Novaya Zemlya’s marine-terminating outlet
395 glaciers between 2000 and 2013. *Cryosphere*, **11**(5), 2149–2174 (doi: 10.5194/tc-11-2149-2017)
- 396 Ciraci E, Velicogna I and Sutterley TC (2018) Mass Balance of Novaya Zemlya Archipelago, Russian High Arctic,
397 Using Time-Variable Gravity from GRACE and Altimetry Data from ICESat and CryoSat-2. *Remote Sens.*, **10**(11),
398 1817 (doi: 10.3390/rs10111817)
- 399 Gorelick N, Hancher M, Dixon M, Ilyushchenko S, Thau D and Moore R (2017) Google Earth Engine: Planetary-scale
400 geospatial analysis for everyone. *Remote Sens. Environ.*, **202**, 18–27 (doi: 10.1016/j.rse.2017.06.031)
- 401 Granshaw FD and Fountain AG (2006) Glacier change (1958-1998) in the North Cascades National Park Complex,
402 Washington, USA. *J. Glaciol.*, **52**(177), 251–256 (doi: 10.3189/172756506781828782)
- 403 Grant KL, Stokes CR and Evans IS (2009) Identification and characteristics of surge-type glaciers on Novaya Zemlya,
404 Russian Arctic. *J. Glaciol.*, **55**(194), 960–972 (doi: 10.3189/002214309790794940)
- 405 Hall DK, Riggs GA and Salomonson VV (1995) Development of methods for mapping global snow cover using
406 moderate resolution imaging spectroradiometer data. *Remote Sens. Environ.*, **54**(2), 127–140 (doi: 10.1016/0034-
407 4257(95)00137-P)
- 408 Hemati M, Hasanlou M, Mahdianpari M and Mohammadimanesh F (2021) A systematic review of landsat data for
409 change detection applications: 50 years of monitoring the earth. *Remote sens.*, **13**(15), 2869

- 410 Hock, R and 7 others (2019) GlacierMIP-A model intercomparison of global-scale glacier mass-balance models and
411 projections. *J. Glaciol.*, **65**(251), 453–467 (doi: 10.1017/jog.2019.22)
- 412 Hugonnet, Romain and 10 others (2021) Accelerated global glacier mass loss in the early twenty-first century. *Nature*,
413 **592**(7856), 726–731 (doi: 10.1038/s41586-021-03436-z)
- 414 IPCC (2021) *Climate Change 2021: The Physical Science Basis. Contribution of Working Group I to the Sixth*
415 *Assessment Report of the Intergovernmental Panel on Climate Change*. Cambridge University Press, Cambridge,
416 United Kingdom and New York, NY, USA
- 417 Isaksen, Ketil and 15 others (2022) Exceptional warming over the Barents area. *Sci Rep*, **12**(1), 9371 (doi:
418 10.1038/s41598-022-13568-5)
- 419 Khan AA, Jamil A, Hussain D, Taj M, Jabeen G and Malik MK (2020) Machine-Learning Algorithms for Map-
420 ping Debris-Covered Glaciers: The Hunza Basin Case Study. *IEEE Access*, **8**, 12725–12734 (doi: 10.1109/AC-
421 CESS.2020.2965768)
- 422 Kochtitzky W and Copland L (2022) Retreat of Northern Hemisphere Marine-Terminating Glaciers, 2000–2020.
423 *Geophys. Res. Lett.*, **49**(3), e2021GL096501 (doi: 10.1029/2021GL096501)
- 424 Kohnemann SHE, Heinemann G, Bromwich DH and Gutjahr O (2017) Extreme Warming in the Kara Sea and
425 Barents Sea during the Winter Period 2000–16. *J. Clim.*, **30**(22), 8913–8927 (doi: 10.1175/JCLI-D-16-0693.1)
- 426 Kulkarni AD and Lowe B (2016) Random Forest Algorithm for Land Cover Classification. *Int. J. Recent Innov.*
427 *Trends Comput. Commun.*, **4**(3), 58–63 (doi: 10.17762/ijritcc.v4i3.1834)
- 428 Kulp SA and Strauss BH (2019) New elevation data triple estimates of global vulnerability to sea-level rise and
429 coastal flooding. *Nat. Commun.*, **10**(1) (doi: 10.1038/s41467-019-12808-z)
- 430 Kumar A, Yadav J and Mohan R (2021a) Spatio-temporal change and variability of barents-kara sea ice, in the
431 arctic: Ocean and atmospheric implications. *Sci. Total. Environ.*, **753**, 142046
- 432 Kumar M, Al-Quraishi AMF and Mondal I (2021b) Glacier changes monitoring in Bhutan High Himalaya using
433 remote sensing technology. *Environ. Eng. Res.*, **26**(1) (doi: 10.4491/eer.2019.255)
- 434 Kääb, A M and 11 others (2005) Remote sensing of glacier- and permafrost-related hazards in high mountains: an
435 overview. *Nat. Hazard Earth Syst. Sci.*, **5**(4), 527–554 (doi: 10.5194/nhess-5-527-2005)
- 436 Lea JM (2018) The google earth engine digitisation tool (geedit) and the margin change quantification tool (maqit)–
437 simple tools for the rapid mapping and quantification of changing earth surface margins. *Earth Surf. Dyn.*, **6**(3),
438 551–561

- 439 Liu, Xiaoping and 7 others (2018) High-resolution multi-temporal mapping of global urban land using Landsat images
440 based on the Google Earth Engine Platform. *Remote Sens. Environ.*, **209**, 227–239 (doi: 10.1016/j.rse.2018.02.055)
- 441 Ma L, Liu Y, Zhang X, Ye Y, Yin G and Johnson BA (2019) Deep learning in remote sensing applications: A meta-
442 analysis and review. *ISPRS J. Photogramm. Remote Sens.*, **152**, 166–177 (doi: 10.1016/j.isprsjprs.2019.04.015)
- 443 Mahdianpari, Masoud and 7 others (2020) Big data for a big country: The first generation of canadian wetland
444 inventory map at a spatial resolution of 10-m using sentinel-1 and sentinel-2 data on the google earth engine cloud
445 computing platform. *Can. J. Remote Sens.*, **46**(1), 15–33
- 446 Masek, Jeffrey G and 6 others (2020) Landsat 9: Empowering open science and applications through continuity.
447 *Remote Sens. Environ.*, **248**, 111968 (doi: 10.1016/j.rse.2020.111968)
- 448 Melkonian AK, Willis MJ, Pritchard ME and Stewart AJ (2016) Recent changes in glacier velocities and thinning at
449 Novaya Zemlya. *Remote Sens. Environ.*, **174**, 244–257 (doi: 10.1016/j.rse.2015.11.001)
- 450 Millan R, Mouginot J, Rabatel A and Morlighem M (2022) Ice velocity and thickness of the world’s glaciers. *Nat*
451 *Geosci*, 1–6 (doi: 10.1038/s41561-021-00885-z)
- 452 Moon, Twila A and 14 others (2019) The Expanding Footprint of Rapid Arctic Change. *Earth’s Future*, **7**(3), 212–218
453 (doi: 10.1029/2018EF001088)
- 454 Nery T, Sadler R, Solis-Aulestia M, White B, Polyakov M and Chalak M (2016) Comparing supervised algorithms
455 in Land Use and Land Cover classification of a Landsat time-series. In *2016 IEEE International Geoscience and*
456 *Remote Sensing Symposium (IGARSS)*, 5165–5168 (doi: 10.1109/IGARSS.2016.7730346)
- 457 Nijhawan R, Garg P and Thakur P (2016) A comparison of classification techniques for glacier change detection
458 using multispectral images. *Perspect. Sci.*, **8**, 377–380 (doi: 10.1016/j.pisc.2016.04.080)
- 459 Nuth, C and 7 others (2013) Decadal changes from a multi-temporal glacier inventory of Svalbard. *Cryosphere*, **7**(5),
460 1603–1621 (doi: 10.5194/tc-7-1603-2013)
- 461 Olofsson P, Foody GM, Stehman SV and Woodcock CE (2013) Making better use of accuracy data in land change
462 studies: Estimating accuracy and area and quantifying uncertainty using stratified estimation. *Remote Sens.*
463 *Environ.*, **129**, 122–131 (doi: 10.1016/j.rse.2012.10.031)
- 464 Paul F (2017) Glacier Inventory. In *International Encyclopedia of Geography*, 1–12, John Wiley & Sons, Ltd, ISBN
465 978-1-118-78635-2 (doi: 10.1002/9781118786352.wbieg0877)
- 466 Paul F, Kääb A, Maisch M, Kellenberger T and Haeberli W (2002) The new remote-sensing-derived Swiss glacier
467 inventory: I. Methods. *Ann. Glaciol.*, **34**, 355–361 (doi: 10.3189/172756402781817941)

- 468 Paul F, Kääb A and Haeberli W (2007) Recent glacier changes in the Alps observed by satellite: Consequences for
469 future monitoring strategies. *Glob. Planet. Chang.*, **56**(1), 111–122 (doi: 10.1016/j.gloplacha.2006.07.007)
- 470 Paul, F and 10 others (2017) Error sources and guidelines for quality assessment of glacier area, elevation change, and
471 velocity products derived from satellite data in the Glaciers_cci project. *Remote Sens. Environ.*, **203**(November),
472 256–275 (doi: 10.1016/j.rse.2017.08.038)
- 473 Paul, F and 24 others (2015) The glaciers climate change initiative: Methods for creating glacier area, elevation
474 change and velocity products. *Remote Sens. Environ.*, **162**, 408–426 (doi: 10.1016/j.rse.2013.07.043)
- 475 Praticò S, Solano F, Di Fazio S and Modica G (2021) Machine Learning Classification of Mediterranean Forest Habi-
476 tats in Google Earth Engine Based on Seasonal Sentinel-2 Time-Series and Input Image Composition Optimisation.
477 *Remote Sens.*, **13**(4), 586 (doi: 10.3390/rs13040586)
- 478 Racoviteanu AE, Arnaud Y, Williams MW and Ordoñez J (2008) Decadal changes in glacier parame-
479 ters in the Cordillera Blanca, Peru, derived from remote sensing. *J. Glaciol.*, **54**(186), 499–510 (doi:
480 10.3189/002214308785836922)
- 481 Racoviteanu AE, Paul F, Raup B, Khalsa SJS and Armstrong R (2009) Challenges and recommendations in mapping
482 of glacier parameters from space: results of the 2008 Global Land Ice Measurements from Space (GLIMS) workshop,
483 Boulder, Colorado, USA. *Ann. Glaciol.*, **50**(53), 53–69 (doi: 10.3189/172756410790595804)
- 484 Rantanen, Mika and 7 others (2022) The Arctic has warmed nearly four times faster than the globe since 1979.
485 *Commun Earth Env.*, **3**(1), 1–10 (doi: 10.1038/s43247-022-00498-3)
- 486 Rastner P, Bolch T, Notarnicola C and Paul F (2013) A comparison of pixel-and object-based glacier classification
487 with optical satellite images. *IEEE J. Sel. Top. Appl. Earth Obs. Remote Sens.*, **7**(3), 853–862
- 488 Rastner P, Strozzi T and Paul F (2017) Fusion of Multi-Source Satellite Data and DEMs to Create a New Glacier
489 Inventory for Novaya Zemlya. *Remote Sens.*, **9**(11), 1122 (doi: 10.3390/rs9111122)
- 490 Raup BH, Racoviteanu AE, Khalsa SJS, Helm C, Armstrong R and Arnaud Y (2007) The GLIMS geospa-
491 tial glacier database: A new tool for studying glacier change. *Glob. Planet. Chang.*, **56**(1-2), 101–110 (doi:
492 10.1016/j.gloplacha.2006.07.018)
- 493 Ren and Malik (2003) Learning a classification model for segmentation. In *Proceedings Ninth IEEE International*
494 *Conference on Computer Vision*, 10–17 vol.1 (doi: 10.1109/ICCV.2003.1238308)
- 495 RGI Consortium (2017) Randolph Glacier Inventory 6.0 (doi: 10.7265/N5-RGI-60)

- 496 Robson BA, Nuth C, Dahl SO, Hölbling D, Strozzi T and Nielsen PR (2015) Automated classification of debris-
497 covered glaciers combining optical, SAR and topographic data in an object-based environment. *Remote Sens.*
498 *Environ.*, **170**, 372–387 (doi: 10.1016/j.rse.2015.10.001)
- 499 Robson BA, Hölbling D, Nuth C, Strozzi T and Dahl SO (2016) Decadal scale changes in Glacier area in the
500 Hohe Tauern national park (Austria) determined by object-based image analysis. *Remote Sens.*, **8**(1) (doi:
501 10.3390/rs8010067)
- 502 Schädel, Christina and 14 others (2018) Divergent patterns of experimental and model-derived permafrost ecosystem
503 carbon dynamics in response to Arctic warming. *Env. Re Lett*, **13**(10), 105002 (doi: 10.1088/1748-9326/aae0ff)
- 504 Shafizadeh-Moghadam H, Khazaei M, Alavipanah SK and Weng Q (2021) Google Earth Engine for large-scale land
505 use and land cover mapping: an object-based classification approach using spectral, textural and topographical
506 factors. *Giscience Remote Sens.*, **58**(6), 914–928 (doi: 10.1080/15481603.2021.1947623)
- 507 Sharp, Martin and 12 others (2014) Remote sensing of recent glacier changes in the Canadian Arctic. In JS Kargel,
508 GJ Leonard, MP Bishop, A Käab and BH Raup (eds.), *Global Land Ice Measurements from Space*, 205–228,
509 Springer Berlin Heidelberg, Berlin, Heidelberg, ISBN 978-3-540-79817-0 978-3-540-79818-7 (doi: 10.1007/978-3-
510 540-79818-7_9)
- 511 Tassi A and Vizzari M (2020) Object-Oriented LULC Classification in Google Earth Engine Combining SNIC, GLCM,
512 and Machine Learning Algorithms. *Remote Sens.*, **12**(22), 3776 (doi: 10.3390/rs12223776)
- 513 Winsvold SH, Andreassen LM and Kienholz C (2014) Glacier area and length changes in Norway from repeat
514 inventories. *Cryosphere*, **8**(5), 1885–1903 (doi: 10.5194/tc-8-1885-2014)
- 515 Wulder, Michael A and 26 others (2022) Fifty years of Landsat science and impacts. *Remote Sens. Environ.*, **280**,
516 113195 (doi: 10.1016/j.rse.2022.113195)
- 517 Xue, Xingyu and 7 others (2018) Delineating Urban Boundaries Using Landsat 8 Multispectral Data and VIIRS
518 Nighttime Light Data. *Remote Sens.*, **10**(5), 799 (doi: 10.3390/rs10050799)
- 519 Yamagami Y, Watanabe M, Mori M and Ono J (2022) Barents-kara sea-ice decline attributed to surface warming in
520 the gulf stream. *Nat. commun.*, **13**(1), 1–10
- 521 You, Qinglong and 15 others (2021) Warming amplification over the Arctic Pole and Third Pole: Trends, mechanisms
522 and consequences. *Earth-science Rev.*, **217**, 103625 (doi: 10.1016/j.earscirev.2021.103625)
- 523 Zemp, M and 14 others (2019) Global glacier mass changes and their contributions to sea-level rise from 1961 to
524 2016. *Nature*, **568**(7752), 382–386 (doi: 10.1038/s41586-019-1071-0)

525 Zhang, Xiao and 6 others (2020) Development of a global 30 m impervious surface map using multisource and
526 multitemporal remote sensing datasets with the google earth engine platform. *Earth Syst. Sci. Data*, **12**(3), 1625–
527 1648